The Plenacoustic Function and its Sampling

Thibaut Ajdler, *Student member, IEEE*, Luciano Sbaiz, Martin Vetterli, *Fellow, IEEE.*

Abstract

We study the spatialization of the sound field in a room, in particular the evolution of room impulse responses as a function of their spatial positions. We observe that the multidimensional spectrum of the solution of the wave equation has an almost bandlimited character. Therefore sampling and interpolation can easily be applied using signals on an array. The decay of the spectrum is studied on both temporal and spatial frequency axes. We study how this decay influences the performance of the interpolation. Based on the support of the spectrum, we determine the number and the spacing between the microphones needed to reconstruct the sound field up to a certain temporal frequency. The optimal sampling pattern for the microphone positions is given for the linear and the planar case. Existing techniques usually make use of room models to recreate the sound field present at some point in the space. Our technique simply starts from the measurements of the sound field in a finite number of positions and with this information the total sound field can be recreated. Finally, simulations and experimental results are presented and compared with the theory.

Index Terms

Plenoptic function, room impulse response, sampling, interpolation, sound field sampling, acoustic echo cancellation.

I. Introduction

Assume you are in a concert hall, and you want to faithfully describe the acoustic experience at any location in the hall. What is the evolution of the sound field over space? And if you record the acoustic

The work presented in this paper was supported by the National Competence Center in Research on Mobile Information and Communication Systems (NCCR-MICS), a center supported by the Swiss National Science Foundation under grant number 5005-67322.

T. Ajdler, L. Sbaiz and M. Vetterli are with the Audiovisual Communications Laboratory, EPFL, Lausanne, Switzerland (e-mail: {thibaut.ajdler, luciano.sbaiz, martin.vetterli}@epfl.ch). M. Vetterli is also with the Dept. of EECS, UC Berkeley, CA 94720.

event with an array of microphones, how many do you need to be able to reproduce the experience at any point?

Conversely, assume a virtual acoustical environment, where sources are moving, while the listener is in a particular spot. How finely do you need to simulate the acoustic impulse response to be able to place the source at any location?

The answers to the above questions, as well as related ones, lie in the spatio-temporal acoustic sound field and its properties. We call this field the *plenacoustic function* (PAF) in reference to the plenoptic function introduced by Adelson and Bergen [1] and which defines "all views in a room". More precisely, the plenoptic function is given by a seven dimensional function, $f(x, y, z, \theta, \Omega, \lambda, t)$ which describes the intensity of the light field seen at location (x, y, z) when looking in direction (θ, Ω), at wavelength λ and time t. Thus, given an acoustic event in a room, we can define the PAF $p(x, y, z, t)$ as the sound recorded at location (x, y, z) and time t[1]. The PAF is the solution of the acoustic wave equation (we chose to give it this particular name referring to the plenoptic function that is the solution of the wave equation for light).

Often, we will be concerned with the case of a single point source. Namely, for a given source S, we denote the room impulse response (RIR) at location (x, y, z) by $h(x, y, z, t)$, and then, if the source generates a signal $s(t)$, the PAF is

$$p(x, y, z, t) = \int_{-\infty}^{\infty} s(\tau) h(x, y, z, t - \tau) \mathrm{d}\tau.$$

When the emitted sound is a Dirac pulse, the PAF becomes simply the spatio-temporal RIR. The PAF is then the Green's function. By the superposition principle, the total sound field can be regarded as the sum of all point sources convolved with their spatio-temporal RIRs.

From the view of the physicist, the PAF is simply the solution of the wave equation with appropriate boundary conditions, and a given driving function. From the point of view of the numerical analyst, the system would be very complex for any reasonable room, even for very simple cases. For the signal processor, acoustic RIRs have been studied, measured and simulated for many scenarios, and it is thus natural to study the PAF globally. A natural question for a signal processor is of course the sampling question: is there a discrete set of points in time and space from which the full PAF can be reconstructed? The equivalent question for the plenoptic function was posed and solved by Chai et al [2] with further results from Zhang et al [3]. For the time dimension, we assume bandlimited sources to allow sampling in

[1]If we use directional microphones, we can add directions θ and Ω as well.

time. The more interesting question is of course sampling in space, which directly relates to the number of microphones necessary to acquire the PAF. Interestingly, it is possible to show that the PAF is essentially bandlimited[2] in space, and this to a spatial frequency ϕ which is related to the temporal frequency ω in a linear manner

$$\phi = \frac{\omega}{c},$$

with c being the sound speed propagation. Thus, if the time domain signal is bandlimited to ω_0, then the spatial frequency is limited to $\frac{\omega_0}{c}$, and the PAF can be sampled with a spatial distance d

$$d = \frac{c\pi}{\omega_0}.$$

For high quality audio, d is quite small (e.g. a sampling frequency of 44.1 kHz corresponds to $d = 0.8$ cm) and thus not necessarily very practical with current technology. For voice quality audio (8 kHz sampling frequency corresponding to $d = 4.5$ cm), the spacing becomes more reasonable. A typical set up for the measurement of the PAF, as well as the spatio-temporal spectrum of the PAF are shown in Fig. 1.

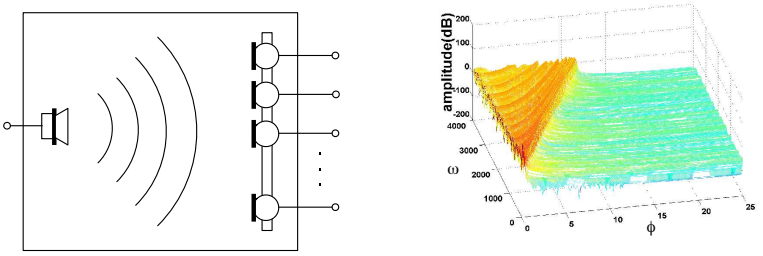

(a) (b)

Fig. 1. Plenacoustic function. (a) Measurement of the PAF. A loudspeaker emits a propagating wave. This sound wave is recorded using an array of microphones. (b) Corresponding spatio-temporal spectrum of the PAF. The axes ϕ and ω are spatial and temporal frequencies, respectively.

The purpose of this paper is to study the characteristics of the PAF in detail, in particular for a room (including air and wall absorption). The key is to derive the essential support of the spatial-temporal frequency response of a room, and to derive decay rates beyond the essential support. Given this characterization, sampling theorems and interpolation formulas can be derived. The results are verified both through simulation experiments and through measurements in actual rooms.

[2]The notion of essentially bandlimited will be made more precise, but means that most of the energy is within the bandlimit.

Beyond the fundamental interest of characterizing precisely the PAF and its sampling, the results are useful in spatial audio applications. For example, it indicates to what extent a microphone array can be used to interpolate any spatial location. Or conversely, how many spatial positions of a source are needed to synthesize arbitrary positions for a virtual source. A further application can be found in acoustic echo cancellation. If a frequency domain adaptive filter is used, the essential triangular support of the spatio-temporal Fourier transform gives an indication of different rates of changes at different temporal frequencies.

The name of the plenacoustic function[3] has been for the first time mentioned in [4]. The first analysis of the function has been given in [5]–[7]. Previous literature exists on the bandlimited character of the solution of the wave equation (acoustic or EM case) along the temporal and spatial frequencies but always under the far field assumption as well as the infinite character of the array [8]. Recently, and in parallel to our work, Coleman [9] has investigated the wide-band electromagnetic impulse response in far field, deriving sampling results under this assumption.

From the knowledge of the PAF in a region of space, extrapolation of the sound field can also be obtained in other regions of space. This is related to wave field synthesis (WFS) [10] and will not be discussed in the present paper. The WFS is based on the Huygens principle stating that the propagation of a wave through a medium can be qualitatively described by adding the contributions of all secondary sources positioned along a wave front. Measuring the sound field on an infinite plane of microphones would allow us to reconstruct the sound field in any point of the source-free half space, which is interesting in a free field situation. Recent techniques have shown interesting results even using 1-dimensional microphone arrays (mostly circular arrays) but limitations occur when trying to extrapolate real 3-dimensional RIRs [11].

The outline of the paper is the following. In Section II, we present the PAF and its construction. Section II-A reminds the reader what RIRs are and how they can be simulated, while Section II-B constructs the space-time representation. Section III studies the spectrum of the PAF on a line in the room. We describe its spatial and temporal frequency decay in Section III-A and III-B respectively. Section IV studies then the sampling of the PAF. We present the sampling of the PAF in Section IV-A followed by a sampling theorem in Section IV-B. With the sampled function, we would like to reconstruct the field in every possible position. This is shown in Section IV-C. Limitations due to the finite length

[3]Remark that the plenacoustic and plenoptic functions are expressions mixing Greek and Latin roots. The Latin expression would be ”the plenaudio function” while the Greek expression would be ”the panacoustic function”.

of the array are taken in account in Section V. The theory presented in this paper is then verified using simulations in Section VI-A and measurements done in real environments in Section VI-B. Section VII is devoted to the generalization of the PAF to multidimensional spatial positions. Different setups are considered: the lines of microphones and loudspeakers in Section VII-A, the plane of microphones in Section VII-B and finally the 3-dimensional space filled of microphones in Section VII-C. Future work is discussed in Section VIII. The conclusions are drawn in Section IX.

II. Construction of the plenacoustic function

To study the sound field along a line of microphones in a room, we need to study the sound field from every possible source position in the room to any possible microphone position on the line. For simplicity we present the technique for a single source but it will be shown later that the technique works as well for multiple sources. Consider a source S emitting a signal $s(t)$. The microphones located on the line will not record exactly $s(t)$. The sound at microphone m_1 is $s(t)$ convolved with the RIR corresponding to the direct path between S and m_1, followed by a possibly infinite number of reflections on the walls (each microphone will receive a sum of delayed and attenuated versions of $s(t)$). At another microphone position m_2, the recorded signal will be different since the RIR from S to m_2 is different than the RIR from S to m_1. The only parameter changing between the different spatial positions is the RIR. Therefore the rest of the analysis of this paper will be focused on the spatial evolution of the RIRs.

A. Modeling the room

In order to calculate the PAF in a room, we need to know the RIRs at any point in the room. We use the image method discussed in [12] for the simulations of RIRs. The method is based on the creation of virtual sources in order to simulate the effect of the reflections on the walls. In the case of a rectangular rigid-walls room of size (L_x, L_y, L_z), the RIRs are given by [12]:

$$p(t, S, M) = \sum_{p=0}^{7} \sum_{v=-\infty}^{\infty} \frac{\delta(t - \|d_p + d_v\|/c)}{4\pi\|d_p + d_v\|}\,, \tag{1}$$

where $d_p = (x_s \pm x_m, y_s \pm y_m, z_s \pm z_m)$, $d_v = (2lL_x, 2nL_y, 2oL_z)$, (l, n, o) being an integer vector triplet and c the speed of sound propagation. The RIR is a function of time and is dependent on the source $S = (x_s, y_s, z_s)$ and the microphone position $M = (x_m, y_m, z_m)$. The first sum shows that in a 3-dimensional field, 7 virtual sources are created in addition to the original source. The second sum shows that sound between two parallel rigid walls is infinitely reverberated. More general formulas taking into account the reflection factors of the walls are given in [12]. One practical limitation of the method is the

quantization rounding in the computation of the RIR. Each image contribution is computed exactly but needs in practice to be rounded to the closest sample in time. This leads to aliasing in time and space. In our simulations, we have replaced each dirac by sinc functions of appropriate bandwidth delayed with the exact non integer delay. This removes the aliasing effect. However, as the sinc functions have a very slow decay in time, one has to consider long enough RIR to allow the sincs to sufficiently vanish.

B. Space time representation

With the RIRs as defined in (1), we construct the PAF for a line in the room. In that case, we can construct a 2-dimensional graph by gathering all the RIRs at any position on the line, leading to a 2-dimensional continuous function of space and time. Space represents the position, time being the duration of the RIR. This representation is shown in Fig. 2(a) when a pulse is recorded on a line of microphones in free field and in Fig. 2(b) for the case of a room.

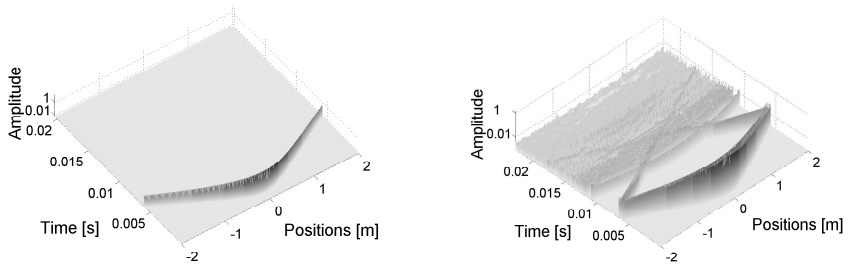

(a) (b)

Fig. 2. PAF in time and space. (a) In free field. (b) Inside a room.

III. Spectrum of the PAF on a line

In this section, we study the PAF on a line and its associate spectrum. We give a analytical expression of 2D-FT of the PAF. Further, the spatial and temporal frequency decay of the spectrum of the PAF are studied.

A. Spatial decay of the spectrum of the PAF

We give an analytical expression for the 2-dimensional Fourier transform (2D-FT) of the PAF. This is first reviewed for the free field case, followed by a general formula in the case of a rectangular room.

1) Free field case: We study the evolution of the RIR along the x-axis. The PAF in space and time domain is given by the following formula [13]:

$$p(x,t) = \frac{\delta(t - \frac{\sqrt{(x-x_s)^2+(y_m-y_s)^2+(z_m-z_s)^2}}{c})}{4\pi\sqrt{(x-x_s)^2+(y_m-y_s)^2+(z_m-z_s)^2}}. \tag{2}$$

We only vary the x component of the microphone. For simplicity, we remove the subscript in the variable x_m, denoting it by x. The variables y_m, z_m, x_s, y_s and z_s are constant. Calling $d^2 = (y_m - y_s)^2 + (z_m - z_s)^2$, we rewrite (2) as

$$p(x,t) = \frac{\delta(t - \frac{\sqrt{(x-x_s)^2+d^2}}{c})}{4\pi\sqrt{(x-x_s)^2+d^2}}. \tag{3}$$

We calculate the spectrum of this function in Appendix I. The obtained result for $\omega \in \mathbb{R}^+$ and $\phi \in \mathbb{R}$ is[4]:

$$P(\phi,\omega) \quad = \quad -\frac{j}{4}e^{-j\phi x_s} H_0^* \left(d\sqrt{(\frac{\omega}{c})^2 - \phi^2} \right), \tag{4}$$

with ϕ and ω being respectively the spatial and temporal frequencies. H_0^* represents the complex conjugate of the Hankel function of order zero. This function is infinite in zero. Therefore when either $d = 0$ or $|\phi| = \frac{\omega}{c}$ the plenacoustic spectrum becomes infinite[5]. The values where $|\phi| > \frac{\omega}{c}$ correspond to the evanescent mode of the waves. The waves lose their propagating character to become exponentially fast decaying waves [14]. Remark also that for $|\phi| \geq \frac{\omega}{c}$, (4) becomes:

$$P(\phi,\omega) \quad = \quad \frac{1}{2\pi}e^{-j\phi x_s} K_0 \left(d\sqrt{\phi^2 - (\frac{\omega}{c})^2} \right), \tag{5}$$

where K_0 is a modified Bessel function of the second kind and order zero. The modified Bessel function of the second kind has the following asymptotical[6] behavior[7] (see [14]):

$$K_0(x) \sim \sqrt{\frac{\pi}{2x}} e^{-x}. \tag{6}$$

[4]Since $p(x,t)$ is a real function, we have that $P(-\phi,-\omega) = P^*(\phi,\omega)$, with P^* the complex conjugate of P. To simplify the notation, all further derivations are done for $\omega \in \mathbb{R}^+$.

[5]$d = 0$ corresponds to the situation where the source is located on the line of the microphones. ϕ is the spatial frequency of the signal captured on the line of microphones. Consider a sinusoid of temporal frequency ω rad/s emitted from a certain position. The signal acquired by the microphones located at positions tending to infinity is at one instant an attenuated sinusoid of spatial frequency $\frac{\omega}{c}$ rad/m. Remark also that for the microphone positions at infinity the source appears as being on the line. In the case of the line of microphones, having a source on the line leads to an infinite spectrum.

[6]$f(x) \sim g(x)$ means that $\lim_{x\to\infty} \frac{f(x)}{g(x)} = 1$.

[7]Further numerical computations show that $K_0(x) \leq \sqrt{\frac{\pi}{2x}} e^{-x}$ for $x > 0$.

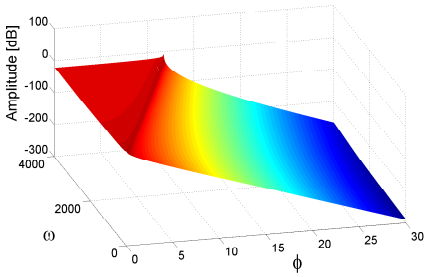

Fig. 3. Theoretical 2D spectrum of the PAF according to (4).

For large ϕ, (5) can be rewritten using (6) as:

$$P(\phi,\omega) \sim \frac{1}{2\pi} e^{-j\phi x_s} \sqrt{\frac{\pi}{2d\sqrt{\phi^2-(\frac{\omega}{c})^2}}} e^{-d\sqrt{\phi^2-(\frac{\omega}{c})^2}}. \tag{7}$$

For a finite $\omega = \omega_0$, (7) asymptotically behaves as:

$$P(\phi,\omega_0) \sim \frac{e^{-j\phi x_s}}{2\sqrt{\pi}} \sqrt{\frac{1}{d\phi}} e^{-d\phi}. \tag{8}$$

We see that the decay along the spatial frequency axis is exponential. Therefore, considering $\omega, \phi \in \mathbb{R}$, most of the energy is contained in the part of the spectrum satisfying

$$|\phi| \leq \frac{|\omega|}{c}. \tag{9}$$

This result will be used later in the sampling of the PAF. As the spectrum is decaying very fast along the spatial frequency axis, we will be able to derive a sampling theorem to sample and reconstruct the PAF along the spatial axis (see Section IV).

2) Rectangular room: In the case of a rectangular room of size (L_x, L_y, L_z), we consider all the reflections as virtual sources as explained in Section II-A and apply the superposition principle. The expression for the PAF is then given by (1). Each virtual source leads to a spectrum that follows (4). The total spectrum of the PAF is the sum of the spectra of each virtual source taken separately, leading to an infinite sum. We would like to know how this sum is decaying for large spatial frequencies.

We present results on the decay of the spatial frequency in the easier case of all the virtual sources located in the plane. Similar results are obtained in the general case of sources located in space.

We use the image model given in Fig. 4. Our original source is s_1 (with coordinates (x_{s_1}, y_{s_1})) and in its immediate neighborhood, we can see 3 other virtual sources (s_2, s_3 and s_4). These 4 mother sources will create an infinite number of repetitions to form all the virtual sources in the plane. These 4 mother sources will be repeated in the x and y direction with a periodicity of $2L_x$ and $2L_y$ respectively.

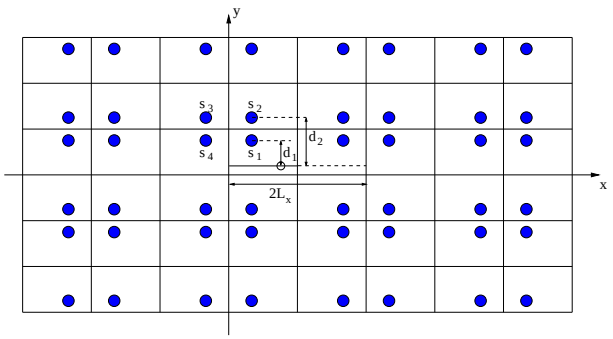

Fig. 4. Image source model with the original source s_1 and all the other virtual sources.

As the room has finite size, we cannot consider an infinite line of microphones. We consider the microphone line to cover the whole length of the room. In Fig. 4, the line is parallel to the x axis.

We define the distances from sources s_1 and s_2 to the line of microphones as d_1 and d_2 respectively (with $d_1 \leq d_2$). The other distances for the sources s_3 and s_4 to the line are in this case also d_1 and d_2.

An interesting aspect of this construction is that by the $2L_x$ periodicity of the source positions along the x axis, the sound recorded on an infinite line is also periodic with period $2L_x$. Further, using the symmetry of the construction, we realize that the sound heard at position ϵ is the same as the one heard at position $2L_x - \epsilon$ with $\epsilon \in [0, L_x]$.

By discretizing the spectrum of the PAF on the ϕ axis, and introducing $\phi_0 = \frac{\pi}{L_x}$, we exactly obtain the Fourier series of the sound field recorded on a line from 0 to $2L_x$ when this sound field is $2L_x$ periodic.

Considering the 4 mother sources (s_1 to s_4) with their periodic repetitions along the x axis, the discrete spectrum of the PAF can be expressed as follows (for large $n\phi_0$):

$$P(n\phi_0, \omega_0) \sim \left(\frac{e^{-jn\phi_0 x_{s_1}}}{2\sqrt{\pi}} + \frac{e^{-jn\phi_0 x_{s_2}}}{2\sqrt{\pi}} \right) \left(\frac{e^{-d_1 n\phi_0}}{\sqrt{d_1 n\phi_0}} + \frac{e^{-d_2 n\phi_0}}{\sqrt{d_2 n\phi_0}} \right).$$

We therefore can write

$$P(n\phi_0, \omega_0) \sim C_1(n) \left(\frac{e^{-d_1 n\phi_0}}{\sqrt{d_1 n\phi_0}} + \frac{e^{-d_2 n\phi_0}}{\sqrt{d_2 n\phi_0}} \right), \tag{10}$$

with $C_1(n)$ a bounded function in n.

Consider now the $2L_y$ periodic repetitions of the sources along the y axis. We call the sources $s_{1,i}$ the sources with coordinates $(x_{s_1}, y_{s_1} + i2L_y)$ and similarly $s_{2,i}$ the sources with coordinates $(x_{s_2}, y_{s_2} + i2L_y)$. Call $D_{1,i}$ the distances between the line of microphones and the sources $s_{1,i}$, and $D_{2,i}$ the distances

between the line of microphones and the sources $s_{2,i}$. We have that

$$\begin{aligned} D_{1,i} &= |d_1 + i2L_y|, \\ D_{2,i} &= |d_2 + i2L_y|. \end{aligned}$$

When considering all the source repetitions in the x and y directions, the spectrum becomes:

$$P(n\phi_0, \omega_0) \sim C_1(n) \sum_{i=-\infty}^{\infty} \left(\frac{e^{-D_{1,i} n\phi_0}}{\sqrt{D_{1,i} n\phi_0}} + \frac{e^{-D_{2,i} n\phi_0}}{\sqrt{D_{2,i} n\phi_0}} \right). \tag{11}$$

The right member of (11) can be rewritten as:

$$C_1(n) \sum_{i=0}^{\infty} \left(\frac{e^{-(d_1+i2L_y)n\phi_0}}{\sqrt{(d_1+i2L_y)n\phi_0}} + \frac{e^{-(d_2+i2L_y)n\phi_0}}{\sqrt{(d_2+i2L_y)n\phi_0}} + \frac{e^{-(d_1'+i2L_y)n\phi_0}}{\sqrt{(d_1'+i2L_y)n\phi_0}} + \frac{e^{-(d_2'+i2L_y)n\phi_0}}{\sqrt{(d_2'+i2L_y)n\phi_0}} \right), \tag{12}$$

with $d_1' = 2L_y - d_1$ and $d_2' = 2L_y - d_2$.

(12) can be upperbounded by

$$C_1(n) \sum_{i=0}^{\infty} \left(\frac{e^{-(d_1+i2L_y)n\phi_0}}{\sqrt{d_1 n\phi_0}} + \frac{e^{-(d_2+i2L_y)n\phi_0}}{\sqrt{d_2 n\phi_0}} + \frac{e^{-(d_1'+i2L_y)n\phi_0}}{\sqrt{d_1' n\phi_0}} + \frac{e^{-(d_2'+i2L_y)n\phi_0}}{\sqrt{d_2' n\phi_0}} \right). \tag{13}$$

Finally, for large n, (13) can be rewritten as

$$\frac{C_2(n)}{1 - e^{-2L_y n\phi_0}} \left(e^{-d_1 n\phi_0} + e^{-d_2 n\phi_0} \right) + \frac{C_2(n) e^{-2L_y n\phi_0}}{1 - e^{-2L_y n\phi_0}} \left(e^{d_1 n\phi_0} + e^{d_2 n\phi_0} \right), \tag{14}$$

with $C_2(n)$ a bounded function in n. Since $d_1 \leq d_2 \leq 2L_y$, asymptotically for large n, the above expression is of the following order[8]:

$$P(n\phi_0, \omega_0) = O(e^{-d_1 n\phi_0}). \tag{15}$$

This shows that for a reverberant room, the decay is exponential when the line of microphones is parallel to a wall[9].

[8] $f(x) = O(g(x))$ means that there are positive constants c and k, such that $|f(x)| \leq cg(x)$, $\forall x \geq k$.

[9] The case where the line of microphones is not covering the whole length of the room is discussed in Section V-A. The case where the line is not parallel to the wall is studied in Appendix IV. There, the line is extended along the periodic repetitions of the room and it is shown that the measured sound field has an exponentially decaying spectrum. The restriction of this infinite line inside the room can then be seen as a windowing as explained in Section V-A.

B. Temporal frequency decay

The study of the temporal frequency decay is of interest to fully characterize the plenacoustic function. Nevertheless, in most cases we deal with sounds that are bandlimited along the temporal frequency due to the bandwidth of the emitters and receivers. Therefore, the results of this section will be briefly presented since they only are interesting from a theoretical point of view. The more detailed analysis of the presented results can be found in [15]. Similarly to Section III-A, we first present results on the temporal frequency decay for the free field case and generalize them further for a rectangular room.

1) Free field: The spectrum of the PAF is given by expression (4). The asymptotic behavior of the Hankel function is given by [14]:

$$H_0(x) \sim \sqrt{\frac{2}{\pi x}} e^{j(x-\pi/4)}. \tag{16}$$

For large ω, (4) can be rewritten using (16) as:

$$P(\phi,\omega) \sim -\frac{j}{2\sqrt{2\pi}} e^{-j(\phi x_s - \pi/4)} \frac{e^{-jd\sqrt{(\frac{\omega}{c})^2-\phi^2}}}{\sqrt{d\sqrt{(\frac{\omega}{c})^2-\phi^2}}}.$$

Considering a finite $\phi = \phi_0$, (4) asymptotically behaves as:

$$P(\phi_0,\omega) \sim -\frac{j\sqrt{c}}{2\sqrt{2\pi}} e^{-j(\phi_0 x_s - \pi/4)} \frac{e^{-jd\frac{\omega}{c}}}{\sqrt{d\omega}}. \tag{17}$$

Therefore we have that

$$P(\phi_0,\omega) \sim \frac{C_3(\omega)}{\sqrt{\omega}}, \tag{18}$$

with $C_3(\omega)$ a bounded function of ω. This last relation shows that the PAF spectrum along the temporal frequency decays as $\frac{1}{\sqrt{\omega}}$.

2) Rectangular room: In the case of a rectangular room, we follow the same construction as in Section III-A.2. Considering the 4 mother sources (s_1 to s_4) in Fig. 4 with their periodic repetitions along the x axis, the discrete spectrum of the PAF can be expressed as follows (for large ω and a finite $n = n_0$):

$$\begin{aligned} P(n_0\phi_0,\omega) &\sim \frac{-je^{j\pi/4}}{2\sqrt{2\pi}} \left(e^{-jn_0\phi_0 x_{s_1}} + e^{-jn_0\phi_0 x_{s_2}}\right) \left(\frac{e^{-jd_1\frac{\omega}{c}}}{\sqrt{d_1\omega}} + \frac{e^{-jd_2\frac{\omega}{c}}}{\sqrt{d_2\omega}}\right) \\ &\sim C_4(n\phi_0) \left(\frac{e^{-jd_1\frac{\omega}{c}}}{\sqrt{d_1\omega}} + \frac{e^{-jd_2\frac{\omega}{c}}}{\sqrt{d_2\omega}}\right), \end{aligned}$$

with $C_4(n\phi_0)$ being independent of ω.

Considering the $2L_y$ periodic repetitions of the sources along the y axis, we obtain:

$$P(n_0\phi_0,\omega) \sim C_4(n\phi_0) \sum_{i=-\infty}^{\infty} \left(\frac{e^{-jD_{1,i}\frac{\omega}{c}}}{\sqrt{D_{1,i}\omega}} + \frac{e^{-jD_{2,i}\frac{\omega}{c}}}{\sqrt{D_{2,i}\omega}}\right).$$

It is shown in Appendix V that this sum converges and that

$$P(n_0\phi_0, \omega) \sim \frac{C(\omega)}{\sqrt{\omega}},$$

with $C(\omega)$ a bounded function of ω. The spectrum of the PAF along the temporal frequency decays as $\frac{1}{\sqrt{\omega}}$ in the case of a rectangular room.

IV. Sampling and Reconstruction

In the previous sections, we have studied the decay of the 2D spectrum of the PAF both along the temporal and the spatial frequency axes. We have observed that the spectrum of the PAF lies on a support that is almost bandlimited. This result is valid for a single source, but also for a finite number of sources (by superposition principle). In the scope of this paper, we are mostly interested in the sampling of the sound field along the spatial axis. As we cannot use any spatial anti-aliasing filter in the spatial direction, the speed of the spatial frequency decay of the 2D spectrum of the PAF is the key factor for the quality of the reconstruction. Along the temporal direction, we are able to filter our signal in the temporal direction in order to avoid aliasing.

In this section, we present the sampling theorem of the PAF where we derive the quality of the reconstruction when sampling the sound field in space. Further, interpolation techniques are discussed in order to reconstruct the signal from the available samples.

A. Plenacoustic Sampling

In order to uniformly sample the PAF along the spatial direction, we consider a uniformly spaced infinite number of impulse responses. We call ϕ_S the spatial sampling frequency defined as $\frac{2\pi}{\Delta x}$ where Δx is the sampling interval between two consecutive positions of the measured impulse responses. Next to the spatial sampling, we also need to sample the RIRs at a certain temporal sampling rate depending on the desired audio bandwidth. We call ω_S the temporal sampling frequency. We have $\omega_S = \frac{2\pi}{\Delta t}$ with Δt the sampling period of the impulse responses.

In the temporal dimension, one can always bandlimit the signal before sampling it in order to avoid aliasing. Along the spatial dimension, no spatial filtering is possible. Therefore we concentrate first on the spatial sampling.

The schematic top view of the spectrum of the PAF is shown in Fig. 5(a). When sampling the PAF along the spatial dimension with a spatial sampling frequency of ϕ_S, repetitions of the spectrum occur as

shown in Fig. 5(b). Considering these spectral repetitions the sound field can perfectly be reconstructed up to ω_0 with

$$\omega_0 = \frac{c\phi_S}{2} = \frac{c\pi}{\Delta x}. \tag{19}$$

Remark that in Fig. 5(b), the region in bold corresponds to the region that is perfectly reconstructed. This means that the lowest spatial frequencies can be reconstructed up to a temporal frequency of $2\omega_0$.

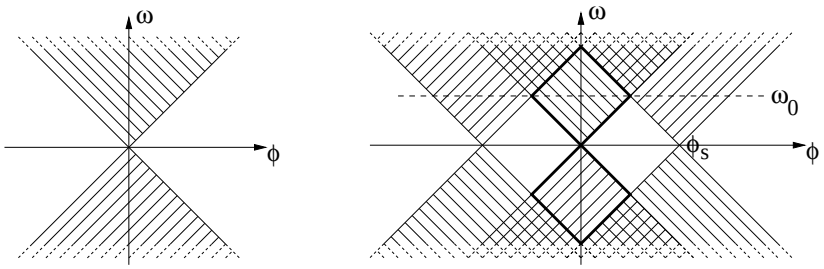

(a) (b)

Fig. 5. PAF spectrum. (a) Top view of the PAF spectrum. (b) Top view of the PAF spectrum with its repetitions due to the spatial sampling. The region in bold corresponds to the region of the spectrum that can be perfectly reconstructed.

We consider now the temporal sampling of the PAF. We first bandlimit the signal to $\omega_0 = \frac{c\phi_S}{2}$ and we sample it with a temporal sampling frequency of $\omega_S = 2\omega_0$. Repetitions of the spectra occur now also along the temporal frequency. The obtained spectrum for the PAF sampled in space and time is shown in Fig. 6(a).

Conversely, by starting the analysis with the temporal sampling, we can say that if the maximal temporal frequency present in the signal is ω_0, then by sampling the signal at a temporal sampling frequency of $\omega_S = 2\omega_0$, we obtain the signal whose spectrum is shown in Fig. 6(b). When we sample this signal along the spatial dimension, it is necessary to choose $\phi_S \geq \frac{2\omega_0}{c}$ in order to avoid aliasing. Fig. 6(a) represents the critical case where $\phi_S = \frac{2\omega_0}{c}$.

The final expression for our sampled PAF 2D spectrum (denoted as P_S) becomes:

$$P_S(\phi,\omega) = \frac{1}{\Delta x \Delta t} \sum_{k_1=-\infty}^{\infty} \sum_{k_2=-\infty}^{\infty} P(\phi - \frac{2\pi k_1}{\Delta x}, \omega - \frac{2\pi k_2}{\Delta t}).$$

B. A Sampling theorem for the PAF

Consider now the spectrum of the PAF at a particular temporal frequency ω_0. It will have the shape given in Fig. 7(a). When the PAF is sampled, repetitions of the spectrum occur as shown in Fig. 7(b).

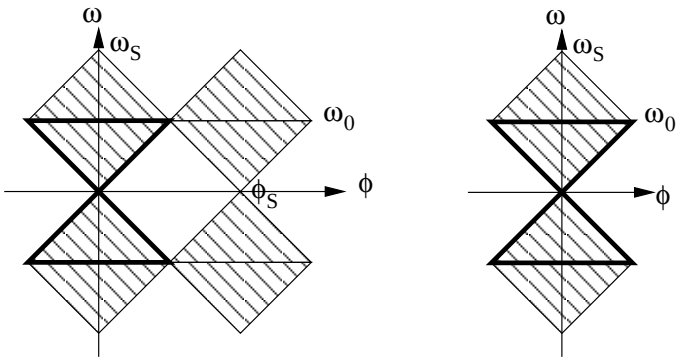

(a) (b)

Fig. 6. PAF spectrum. (a) PAF spectrum with its spectral repetitions along the temporal and the spatial frequencies. (b) PAF spectrum with its spectral repetitions along the temporal frequencies. In both figures, the region in bold corresponds to the original spectrum bandlimited along the temporal frequency without spectral repetitions.

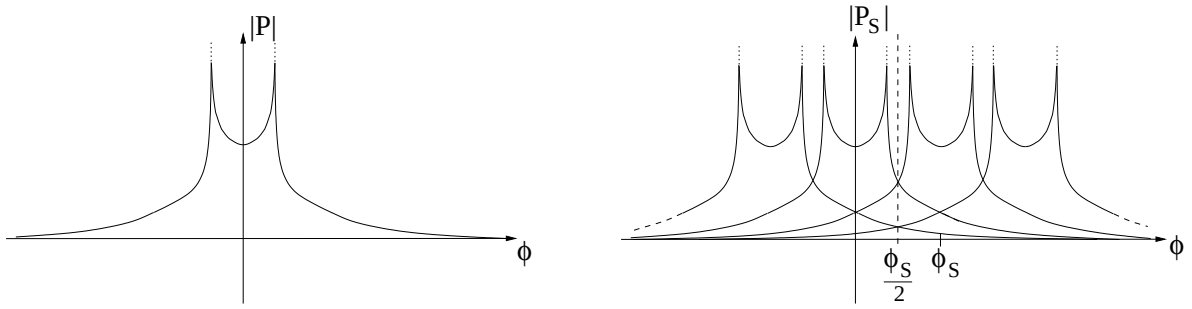

(a) (b)

Fig. 7. Magnitude of the spectrum of the PAF. (a) Cut of the spectrum of the PAF for a particular temporal frequency. (b) Sampled spectrum of the PAF with its spectral repetitions for a particular temporal frequency.

As the spectrum is not perfectly bandlimited, the repetitions will affect the reconstruction. We present a theorem that quantifies the SNR of the reconstruction of the PAF for one source emitting in free field. Call SNR(ϕ_N, ω_0) the SNR of the reconstruction for a sinusoid emitted at frequency $\omega = \omega_0$ with the microphones positioned with a spatial sampling frequency $\phi_S = 2\phi_N$. In the present case, we define the SNR as follows:

$$\text{SNR}(\phi_N, \omega_0) = \frac{\int_{\phi=-\infty}^{\infty} \|P(\phi, \omega_0)\|^2 \mathrm{d}\phi}{4 \int_{\phi=\phi_N}^{\infty} \|P(\phi, \omega_0)\|^2 \mathrm{d}\phi}. \tag{20}$$

The numerator in (20) corresponds to the energy of the spectrum of the PAF at temporal frequency ω_0. The denominator in (20) corresponds to the energy contained in the spectral repetitions that will

contaminate the reconstruction in the spectral domain of interest[10].

Theorem:

Assume one single source emitting in free field at a frequency $\omega = \omega_0$. When sampling the 2D spectrum of the PAF at a spatial sampling frequency of $2\phi_N$, for a particular $\omega = \omega_0$, and reconstructing it using an ideal interpolator, the SNR of the reconstructed signal in the band $[-\phi_N, \phi_N]$ can be expressed as

$$\text{SNR}(\phi_N, \omega_0) = \frac{1}{2d\int_{\phi=\phi_N}^{\infty} H_0^2(d\sqrt{(\frac{\omega_0}{c})^2 - \phi^2})\mathrm{d}\phi}. \tag{21}$$

When considering $\phi_N > \frac{\omega_0}{c}$, the SNR can be lowerbounded:

$$\text{SNR}(\phi_N, \omega_0) \geq \frac{\pi}{4E_i\left(2d\sqrt{\phi_N^2 - \frac{\omega_0}{c}^2}\right)}, \tag{22}$$

where $E_i(\cdot)$ represents the exponential integral function.

Proof:

The numerator in (20) can be rewritten using the Parseval relation as follows:

$$2\pi \int_{x=-\infty}^{\infty} \|\tilde{p}(x, \omega_0)\|^2 \mathrm{d}x,$$

with $\tilde{p}(x, \omega_0)$ the inverse Fourier transform of $P(\phi, \omega_0)$ along the spatial axis. We have that $\tilde{p}(x, \omega_0) = \frac{e^{-j\frac{\omega_0\sqrt{x^2+d^2}}{c}}}{4\pi\sqrt{x^2+d^2}}$, and therefore the numerator in (20) is

$$\frac{2\pi}{16\pi^2} \int_{x=-\infty}^{\infty} \frac{1}{x^2 + d^2} \mathrm{d}x = \frac{1}{8d}. \tag{23}$$

Using (4) and (23) in (20) leads to (21).

When considering $\phi_N > \frac{\omega_0}{c}$, the denominator in (20) is

$$\frac{1}{\pi^2} \int_{\phi=\phi_N}^{\infty} K_0^2\left(d\sqrt{\phi^2 - (\frac{\omega_0}{c})^2}\right) \mathrm{d}\phi.$$

Using the fact that $K_0^2(d\sqrt{\phi^2 - (\frac{\omega_0}{c})^2}) \leq \frac{\pi}{2}\frac{e^{-2d\sqrt{\phi^2-(\frac{\omega_0}{c})^2}}}{d\sqrt{\phi^2-(\frac{\omega_0}{c})^2}}$, we can upperbound the denominator as follows:

$$\frac{1}{2\pi} \int_{\phi=\phi_N}^{\infty} \frac{e^{-2d\sqrt{\phi^2-(\frac{\omega_0}{c})^2}}}{d\sqrt{\phi^2 - (\frac{\omega_0}{c})^2}} \mathrm{d}\phi = \frac{1}{2\pi d} \int_{z=\sqrt{\phi_N^2-(\frac{\omega_0}{c})^2}}^{\infty} \frac{e^{-2dz}}{\sqrt{z^2 + (\frac{\omega_0}{c})^2}} \mathrm{d}z, \tag{24}$$

[10]In the denominator, two different kinds of energy are present: the "in band" and the "out of band" energy. The "in-band" energy corresponds to the energy of all the spectral repetitions in the domain of interest, namely $[-\phi_N, \phi_N]$. The "out of band energy" is the energy present in the spectrum that is outside of the domain of interest. It can be shown that the "in-band" and the "out of band" energies are equal in the case of an infinite line of microphones.

where the equality is obtained with the change of variable $z = \sqrt{\phi^2 - (\frac{\omega_0}{c})^2}$. The right expression in (24) can again be upperbounded as follows:

$$\frac{1}{2\pi d}\int_{z=\sqrt{\phi_N^2-(\frac{\omega_0}{c})^2}}^{\infty}\frac{e^{-2dz}}{z}\mathrm{d}z = \frac{1}{2\pi d}E_i\left(2d\sqrt{\phi_N^2-(\frac{\omega_0}{c})^2}\right), \tag{25}$$

where E_i represents the exponential integral function. Using (25) and (23), we obtain (22). ■

We have computed numerically the SNR in function of different Nyquist frequencies denoted as ϕ_N. This has been done for different temporal frequencies ranging from 1 rad/s to 8000 rad/s. In order to avoid numerical instability due to the infinite value of the spectrum at the position $\phi_N = \frac{\omega}{c}$, our simulations start for each ω at a value $\phi_N = \frac{\omega}{c} + \epsilon$ where ϵ is a very small value (e.g. 0.1 $\frac{rad}{m}$). The results are shown in Fig. 8 together with the lowerbound obtained in (22). We can observe as expected that the SNR increases for larger ϕ_N. Note that the lowerbound follows tightly the SNR obtained numerically.

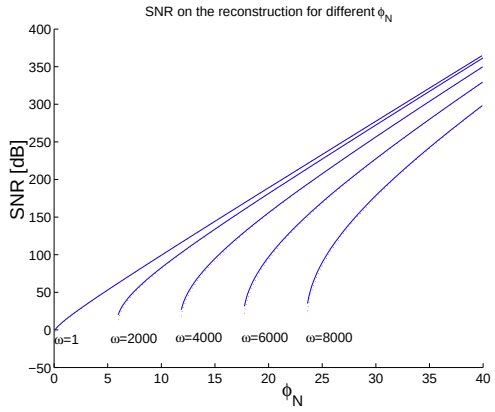

Fig. 8. In full lines, SNR on the reconstruction signal for different ϕ_N for temporal frequencies ranging from 1 rad/s to 8000 rad/s. In dotted line, corresponding SNR lower bounds.

Instead of considering the SNR at a specific temporal frequency, we can easily use the previous result to give the SNR on the reconstruction when the signal is in a frequency band $[\omega_1, \omega_2]$ with spectral characteristics $\beta(\omega)$. The SNR on the reconstruction is given by the following formula:

$$\mathrm{SNR}(\omega_1,\omega_2,\phi_N) = \frac{\int_{\omega=\omega_1}^{\omega_2}\beta^2(\omega)\mathrm{d}\omega}{2d\int_{\omega=\omega_1}^{\omega_2}\beta^2(\omega)\left(\int_{\phi=\phi_N}^{\infty}H_0^2(d\sqrt{(\frac{\omega}{c})^2-\phi^2})d\phi\right)\mathrm{d}\omega}. \tag{26}$$

When considering $\phi_N > \frac{\max(\omega_1,\omega_2)}{c}$, (26) can be lowerbounded as follows:

$$\mathrm{SNR}(\omega_1,\omega_2,\phi_N) \geq \frac{\pi\int_{\omega=\omega_1}^{\omega_2}\beta^2(\omega)\mathrm{d}\omega}{4\int_{\omega=\omega_1}^{\omega_2}\beta^2(\omega)E_i\left(2d\sqrt{\phi_N^2-(\frac{\omega}{c})^2}\right)\mathrm{d}\omega}. \tag{27}$$

Generalization of the sampling theorem for the cases of multiple sources in free field or inside a room is matter of current research.

C. Reconstruction by interpolation

Knowing the sound field at every point of the sampling grid, we apply usual interpolation techniques [16] in order to reconstruct the sound field at any location. First, we need to upsample our time domain signal accordingly to the desired location. We then filter the upsampled PAF with an appropriate 2-dimensional filter. The value at the location of interest is then obtained by interpolation. The interpolation filter to be used is dependent on the sampling grid, and maybe separable in time and space.

1) Rectangular sampling: In the case of rectangular sampling, we just sample the PAF in time and space domain with the sampling grid shown in Fig. 9(a). Convolution of the sampling grid with the spectrum of the PAF leads to Fig. 9(b). In this figure, we can also see the filter needed for interpolation, namely a rectangular filter. In Fig. 9(b) we observe that the spatial sampling frequency is $2\phi_N$. Thus, the interpolation filter is a lowpass with support $[-\phi_N, \phi_N]$. The corresponding spacing between the samples (or microphones) on the spatial axis is $\Delta x = \frac{2\pi}{2\phi_N} = \frac{\pi}{\phi_N}$.

2) Quincunx sampling: A tighter packing of the spectrum can be achieved by using quincunx sampling. In time domain, the grid to be used is shown in Fig. 9(c). In the corresponding spectrum, the spectral repetitions are placed such that they fill the whole frequency space as shown in Fig. 9(d). In this case the filter used for interpolation is a fan filter [3], [17]. The filter is shown in Fig. 9(d). In the quincunx sampling the spatial sampling frequency is now only ϕ_N. This corresponds to a distance between two samples on the space axis of $2\Delta x = \frac{2\pi}{\phi_N}$. This shows that using quincunx sampling we only need to sample the even microphones at even times while the odd microphones are sampled at odd times. This leads to a gain of factor 2 in the processing. However it does not reduce the number of necessary microphones. Similar results have been obtained in [18] in the study of the far field electromagnetic field.

V. Finite Length Aperture

In this section, we do not measure the field along an infinite line but on a finite interval inside the room. This can be seen as a windowing of the PAF in the spatial domain. Consider a rectangular window $w(x)$. In our case, the window is simply a function of the spatial position. Calling the windowed PAF $q(x,t)$, we have $q(x,t) = p(x,t)w(x)$. In frequency domain this is written as

$$Q(\phi,\omega) = P(\phi,\omega) * W(\phi,\omega) = P(\phi,\omega) * (W(\phi)\delta(\omega)) .$$

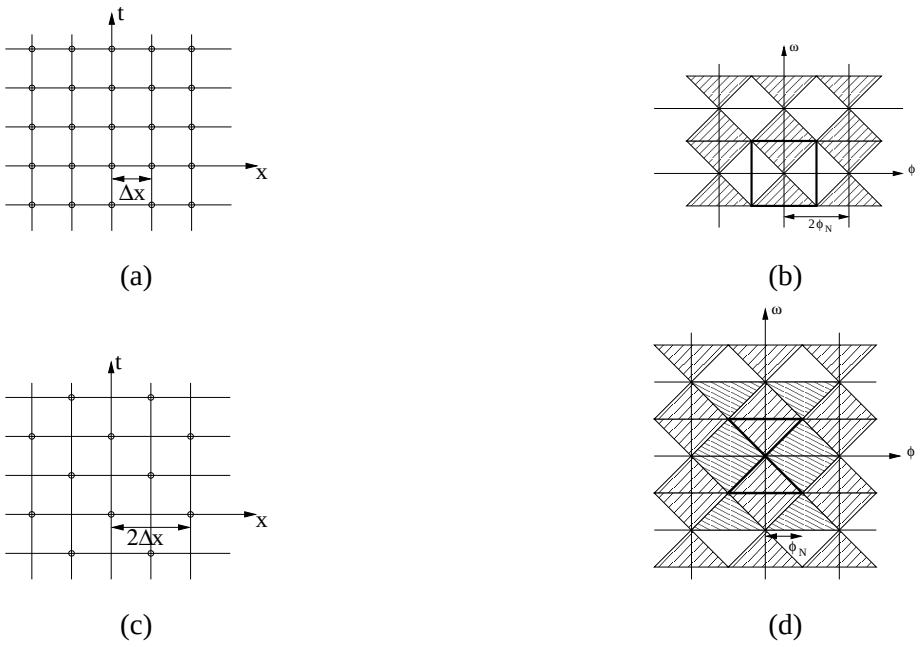

Fig. 9. Sampling of the PAF. (a) Rectangular sampling grid. (b) Plenacoustic spectrum with its repetitions for a rectangular sampling grid. (c) Quincunx sampling grid. (d) Plenacoustic spectrum with its repetitions for a quincunx sampling grid.

The situation is schematically shown in Fig. 10.

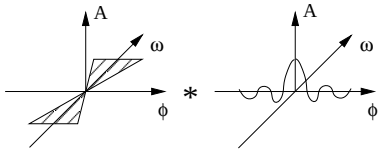

Fig. 10. Effect of the windowing due to the finite length of the array.

A. Aperture size

We now look at the effect of the size of the aperture. Taking measurements from positions between $-\frac{L}{2}$ and $\frac{L}{2}$ leads to a convolution of the PAF spectrum with the following sinc function.

$$W(\phi) = \int_{x=-\frac{L}{2}}^{\frac{L}{2}} e^{-j\phi x} \mathrm{d}x = L\mathrm{sinc}(\frac{\phi L}{2\pi}). \tag{28}$$

We therefore see that at a given ϕ, the larger the value of L, the faster the decay will be. This fact can be observed in Fig. 11. We present a section of the 2D spectrum of the PAF at a particular temporal

frequency. One can observe that for larger aperture sizes the spectrum decays more rapidly as given in (28).

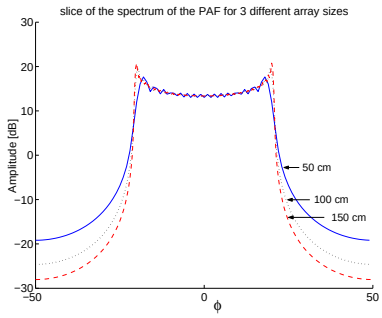

Fig. 11. A section of the PAF at a particular temporal frequency. The curves represent data acquired on intervals of different lengths: 50 cm (full line), 100 cm (dotted line) and 150 cm (dashed line). One can see that a larger interval leads to a faster decay.

The decay of the spectrum of the PAF along the spatial frequency will now be slower than the one in (5). For a particular temporal frequency $\omega = \omega_0$, the decay is:

$$Q(\phi, \omega_0) \quad = \quad \frac{1}{2\pi} e^{-j\phi x_s} K_0 \left(d\sqrt{\phi^2 - (\frac{\omega_0}{c})^2} \right) * W(\phi). \tag{29}$$

In the case of a rectangular window, this decay is the convolution of a sinc with an exponentially decaying function.

Combining the finite aperture effect with the sampling of the PAF, we obtain the following expression for the 2D-FT of the sampled windowed PAF (denoted as Q_S):

$$Q_S(\phi, \omega) = \frac{1}{\Delta x \Delta t} \sum_{k_1=-\infty}^{\infty} \sum_{k_2=-\infty}^{\infty} Q(\phi - \frac{2\pi k_1}{\Delta x}, \omega - \frac{2\pi k_2}{\Delta t}).$$

In the situation of Section III-A.2 considering an infinite number of sources introduced by reflections following the model in [12], the spatial frequency decay of the sampled spectrum is:

$$Q(n\phi_0, \omega) \quad = \quad P(n\phi_0, \omega) * W(n\phi_0), \tag{30}$$

where $W(n\phi_0) = L\text{sinc}(\frac{nL}{2L_x})$. Combined with the sampling of the sound field, the sampled windowed discrete spectrum is[11]:

$$Q_S(n\phi_0, \omega) = \frac{1}{\Delta x \Delta t} \sum_{k_1=-\infty}^{\infty} \sum_{k_2=-\infty}^{\infty} Q(n\phi_0 - \frac{2\pi k_1}{\Delta x}, \omega - \frac{2\pi k_2}{\Delta t}).$$

[11]For simplicity, we give the expression considering that $2L_x$ is a multiple of Δx.

B. Position of the spatial window

We present some results on the shape of the spectrum of the PAF depending on the relative position of the source with respect to the spatial window. In the special case of Fig. 12(a), the spatial window is on the far side of the source. The 2D-FT of the PAF has then the very specific shape shown in Fig. 12(b). This can be explained by the fact that the 2D-FT of a function $p(x,t) = f(x)\delta(\frac{x}{c} - t)$ is $P(\phi,\omega) = F(\phi + \frac{\omega}{c})$. In our specific case the PAF is still multiplied by the window function (of size L) as shown in Fig. 12(a) and therefore the spectrum of the PAF is then convolved with the Fourier transform of the window function. For different setups of spatial windows and source (see Fig. 12), the shape of the PAF spectrum can change but the support is always essentially given by (9). Note that in free field, when the source is symmetrically located with respect to the spatial window as in Fig. 12(e), a symmetric spectrum is obtained (see Fig. 12(f)).

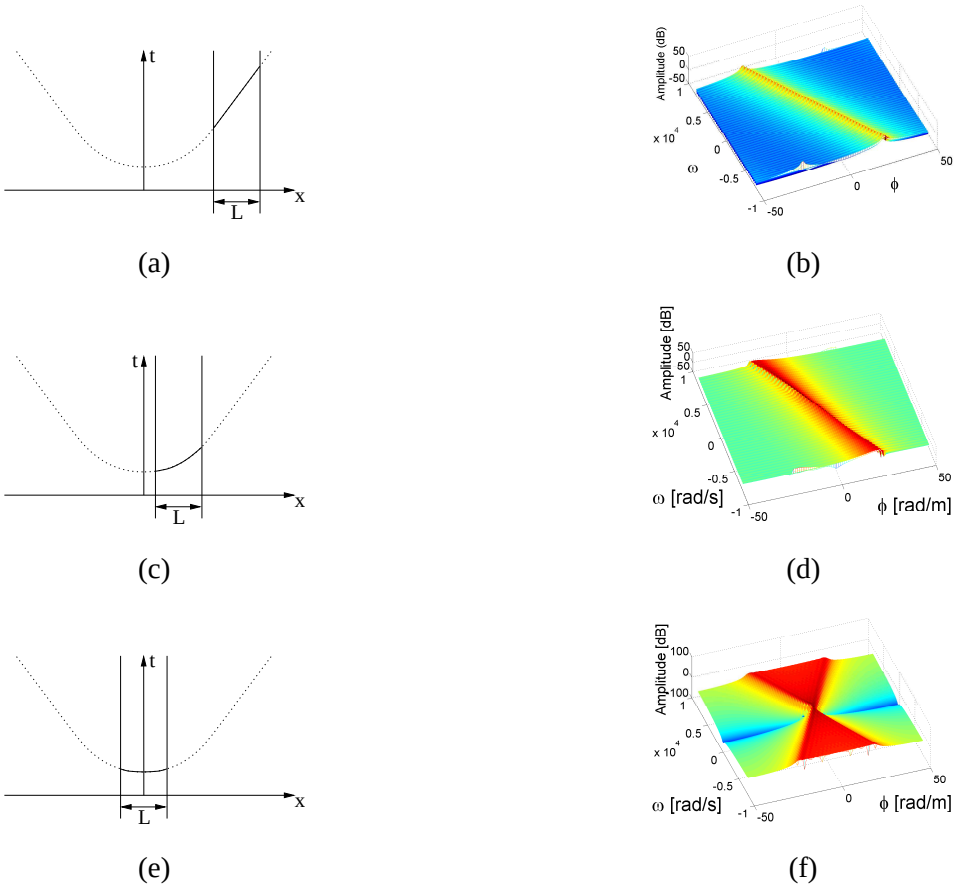

Fig. 12. Top view of PAFs in time and space with their corresponding 2D-FT for different positions of the microphones line with respect to the source position.

VI. Simulations and Measurements

In this section, we present simulation results on the interpolation of RIRs. These results are further compared with real measurements.

A. Simulation results

We have simulated RIRs on a line in a room using the image source model. For simulation purposes, we derive a dense set of impulse responses, keep a subset, and interpolate the missing ones. To compare the obtained results with the simulated RIRs, we use the normalized mean square error (MSE) criterium given by the following formula:

$$\text{MSE} = \frac{\sum_{i=1}^{N} \left(r[i] - \hat{r}[i]\right)^2}{\sum_{i=1}^{N} r^2[i]}, \tag{31}$$

with N the length in samples of the simulated RIRs, r the simulated RIR and $\hat{r}$ the interpolated RIR. In the following figures, the interpolation error is only shown for the positions that were removed. Fig. 13 shows for different lengths of the array the MSE for the reconstructed signals. The RIRs were sampled at $44.1\ kHz$ and simulated every cm. We can observe that using an array of 144 microphones leads to

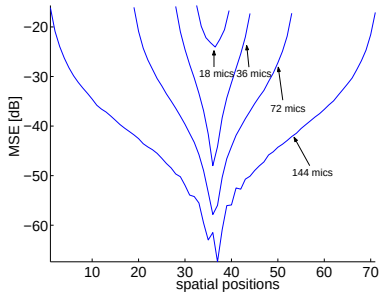

Fig. 13. Interpolation error for different array sizes. We use the same spacing between the microphones.

a very small error (less than -60 dB) for the interpolation in the middle of the array. When using the same spacing between the microphones but reducing the number of RIRs, we observe an increase in the interpolation error. This is shown for different sizes of the array in Fig. 13.

B. Experimental results

Experimental results were carried out in a partially sound insulated room where we measured RIRs at different spatial positions. We used one loudspeaker (Genelec 1029A) and a microphone array (composed of 8 Panasonic $WM61A$). We used a logarithmic sweep [19] to measure the RIRs. We measured 72

RIRs with a spacing of 2 cm. The spectrum of the measured PAF is shown in Fig. 14(a). Using every other RIR we recreated the whole data set. The MSE on the 36 interpolated RIRs measurements is shown in Fig. 14(b). The MSE shown in Fig. 14(b) is obtained when using only the 3000 first samples of the

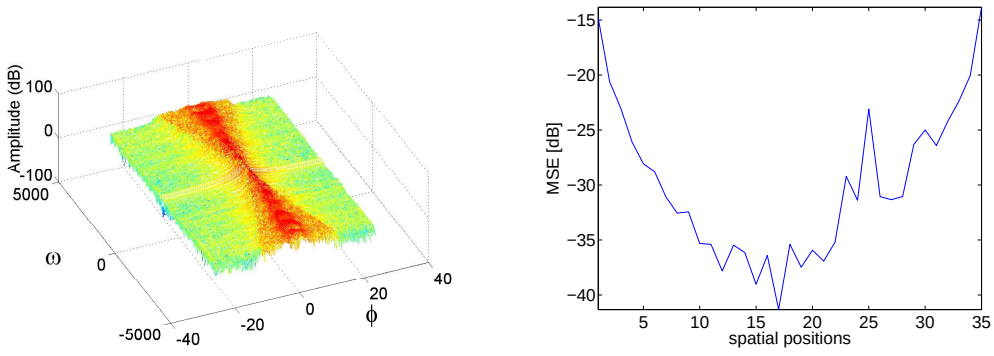

(a) (b)

Fig. 14. Experimental PAF. (a) 2D-FT of the measured plenacoustic function. (b) Interpolation error on measured RIRs.

RIRs. When considering the full RIRs, poorer results are obtained (on the order of -20 to -25 dB). The reason is that in a room, one can observe fluctuations of the temperature. As given in [20], we know that the speed of sound propagation c is proportional to the squared root of the temperature

$$c \approx 20.03\sqrt{273.15 + T_c}, \tag{32}$$

with T_c the temperature in Celsius. In a room, fluctuation of the temperature is very usual due to the presence of outside elements (measurement equipment, computers,...). The effect of temperature changes causes an effect on RIRs due to the change of sound speed propagation. This effect will be the most severe for waves traveling over a wider area. Therefore, the reverberant part of the RIRs undergoes the largest relative timing changes. It is shown in [20] that a variation of 0.1° can create a misalignment between RIRs of more that 25dB. Further, for a fixed microphone position we observed that by repeating the same RIR measurement 100 times in a row, the MSE between the measurement and a reference one (e.g. the first measurement) increased over time. The MSE is of the order of -25 dB after 100 measurements when considering the whole RIR while it of the order of -40 dB when considering only the first 3000 samples. This indicates us that our experimental results can be explained by the fluctuations in temperature.

Remark that due to the limit of our 8 inputs microphone array, we had to move the array to the next positions in order to measure the 72 RIRs (our intrusion in the room probably modified greatly

the temperature field between two sets of measurements). Better results would be obtained if all the measurements could be captured simultaneously, which was not possible due to hardware limitations.

VII. Plenacoustic function for multidimensional spatial positions

The previous sections were devoted to the detailed study of the sampling and interpolation of the sound field on the line. This study can obviously be generalized to other spatial positions of the microphones and loudspeakers. Therefore, we want to study the shape of spectra associated with different microphones and loudspeakers setups. In Section VII-A, we consider a line of loudspeakers emitting in free field and recorded on a line of microphones. Section VII-B studies the spectrum of the PAF associated to a plane of microphones. Optimal sampling patterns for positioning the microphones is also studied. Finally the 3-dimensional space filled of microphones is presented in Section VII-C.

Due to lack of space, these different setups are analyzed in less details than the line of microphones. Temporal and spatial decay analysis in rooms as well as spatial windowing are not presented but can be generalized from the study of the line of microphones.

A. Lines of microphones and loudspeakers

Consider a continuous line of loudspeakers emitting sound in free field. The sound field is recorded by a continuous line of microphones. The lines are parallel to the x axis. The x coordinates of the microphones and loudspeakers are x_m and x_s respectively. For one fixed loudspeaker position x_s, the free field impulse responses associated to the microphone line are $h(x_s - x_m, t)$ with

$$h(x_m - x_s, t) = \frac{\delta(t - \frac{\sqrt{(x_m-x_s)^2+(y_m-y_s)^2+(z_m-z_s)^2}}{c})}{4\pi\sqrt{(x_m - x_s)^2 + (y_m - y_s)^2 + (z_m - z_s)^2}}. \tag{33}$$

Consider now an excitation function $S(x_s, t)$ giving for each position x_s the signal to be emitted. The sound heard on the microphone line is:

$$p(x_m, t) = \int_{x_s=-\infty}^{\infty} \int_{\tau=-\infty}^{\infty} h(x_m - x_s, \tau) S(x_s, t - \tau) \mathrm{d}\tau \mathrm{d}x_s. \tag{34}$$

Taking the 2D-FT of this expression gives

$$P(\phi_x, \omega) = H(\phi_x, \omega) S(\phi_x, \omega), \tag{35}$$

where ϕ_x corresponds to the spatial frequency of the microphone positions. $P(\phi_x, \omega)$ represent the 2D-FT spectrum of the sound heard at the microphone positions, $H(\phi_x, \omega)$ is the 2D spectrum of the impulse responses as given by (4) and $S(\phi_x, \omega)$ is the 2D-FT of the excitation function.

B. Plenacoustic function on a plane

1) Study of the spectrum: In Section III, we studied the shape and the properties of the PAF on a line in the room. In this section, we consider a more general case where the RIRs are studied on a plane. Consider a plane in the space filled with receivers in the x and the y directions. Further, a source is located at position (x_s, y_s, z_s). We know that at any receiver position (x_m, y_m, z_m) the direct path coming from the source is

$$p(x_m, y_m, t) = \frac{\delta(t - \frac{a}{c})}{4\pi a}, \tag{36}$$

with $a = \sqrt{(x_m - x_s)^2 + (y_m - y_s)^2 + (z_m - z_s)^2}$. Calculating the 3D-FT of (36) is done in Appendix II. The result is:

$$P(\phi_x, \phi_y, \omega) = \begin{cases} \frac{-j}{2} e^{-j(\phi_x x_s + \phi_y y_s)} \frac{e^{-j|z_m - z_s|\sqrt{(\frac{\omega}{c})^2 - \phi_q^2}}}{\sqrt{(\frac{\omega}{c})^2 - \phi_q^2}} & \text{for} \quad |\phi_q| \leq \frac{\omega}{c} \\ \frac{1}{2} e^{-j(\phi_x x_s + \phi_y y_s)} \frac{e^{-|z_m - z_s|\sqrt{\phi_q^2 - (\frac{\omega}{c})^2}}}{\sqrt{\phi_q^2 - (\frac{\omega}{c})^2}} & \text{for} \quad \frac{\omega}{c} \leq |\phi_q|. \end{cases} \tag{37}$$

with $\phi_q^2 = \phi_x^2 + \phi_y^2$. Note that ϕ_x and ϕ_y represent the spatial frequencies for the microphones in the x and y directions respectively. The obtained spectrum has a conical shape as shown in Fig. 15. The size

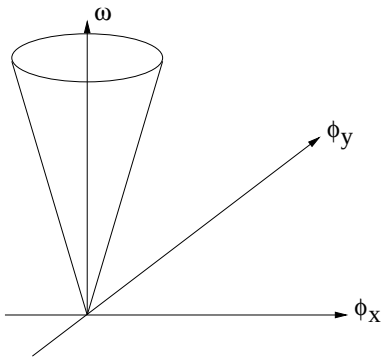

Fig. 15. Scheme for the 3-dimensional spectrum of the PAF.

of the circle follows the following rule:

$$\frac{\omega}{c} = \sqrt{\phi_x^2 + \phi_y^2}. \tag{38}$$

Similarly to the results obtained with the line of microphones, we see that the decay of the spectrum is also exponential outside of the conical shape[12].

[12]Remark that in the specific case of the source located on the plane of the microphones, the decay becomes slower and is, up to a constant, asymptotic to $\frac{1}{\phi_q}$.

2) Optimal sampling pattern: Similarly to the analysis presented in Section IV-C, we study the optimal sampling pattern for the positioning of the microphones on the plane. The first approach is to use the rectangular sampling as shown in Fig. 16(a). We use a spacing Δx_1 and Δy_1 for the spacing between the microphones in the x and y directions. Fig. 16(b) shows the corresponding packing of the circles in the Fourier spectrum for one temporal frequency (typically the highest frequency present in the emitted signal).

The conical shape of the spectrum allows us to obtain a tighter packing of the circles. The use of an hexagonal sampling pattern leads to a reduction of about 15% in the number of necessary microphones. Fig. 16(c) shows the new positions of the microphones on the plane. In our case,

$$\Delta x_2 = \frac{2}{\sqrt{3}} \Delta x_1 \,, \;\; \Delta y_2 = \Delta y_1.$$

Fig. 16(d) shows the corresponding spectrum with its spectral repetitions. Other packings of the cones

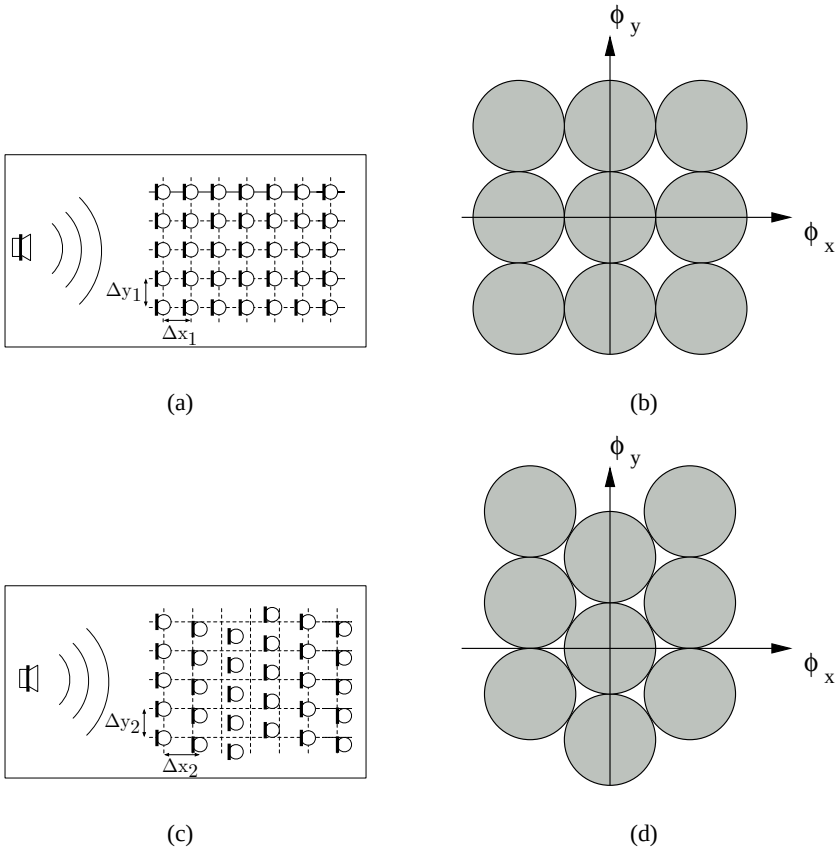

Fig. 16. Sampling of the PAF on a plane. (a) Placement of the microphones on the plane on a rectangular sampling grid. (b) Plenacoustic spectrum with its repetitions for a rectangular sampling grid. (c) Hexagonal sampling grid. (d) Plenacoustic spectrum with its repetitions for a hexagonal sampling grid.

can be realized to lower the temporal sampling frequency of the A/D converters but do not reduce further the number of microphones needed to sample the sound field on a plane [9].

3) Simulation Results: We simulated RIRs on a plane in a room using the image source model. We took the 3-dimensional Fourier transform of the gathered data. By looking at sections of this spectrum for $\omega = 1500$ rad/s and $\omega = 3000$ rad/s, we obtain respectively Fig. 17(a) and (b). We can see that with growing temporal frequencies, the support of the PAF spectrum also increases as given by (38).

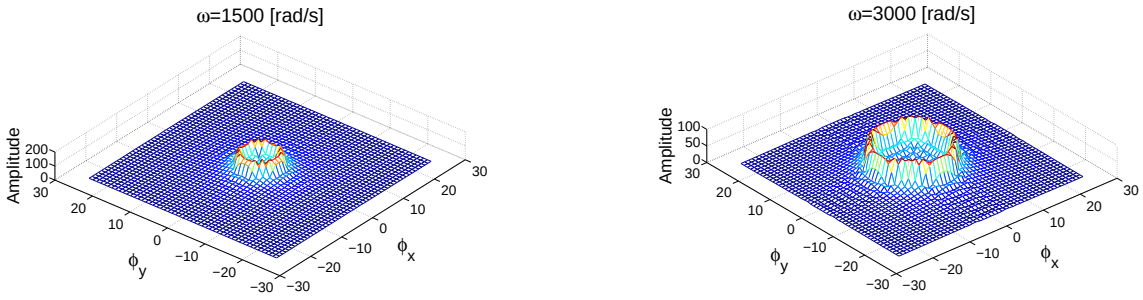

(a) (b)

Fig. 17. Spectrum of the PAF obtained by simulations at different temporal frequencies. (a) $\omega = 1500$ rad/s. (b) $\omega = 3000$ rad/s.

C. Plenacoustic function in space

In this section we consider microphones located in the 3-dimensional space. Similarly to the setup presented in Section VII-B, a source is located at position (x_s, y_s, z_s) and microphones at positions (x_m, y_m, z_m). The PAF is also given by (36). Note that in the present setup also z_m is a variable. We also introduce ϕ_z as the spatial frequency of the microphone positions in the z direction. Calculating the 4D-FT of (36) is done in Appendix III. The result is:

$$P(\phi_x, \phi_y, \phi_z, \omega) = \frac{e^{-j(\phi_x x_s + \phi_y y_s + \phi_z z_s)}}{\phi_x^2 + \phi_y^2 + \phi_z^2 - (\frac{\omega}{c})^2}. \tag{39}$$

(39) represents a cone in 4 dimensions. For a particular temporal frequency, the section of this cone is a sphere[13]. The size of the sphere obeys the following rule:

$$\frac{\omega}{c} = \sqrt{\phi_x^2 + \phi_y^2 + \phi_z^2}. \tag{40}$$

At a particular temporal frequency, the optimal packing of the spheres is given by face-centered cubic lattice packing [21]. It allows to reduce the number of samples by a factor of about 29.3%.

[13]Remark that the decay outside of the sphere is not exponential as was for the plane and line of microphones. This is due to the presence of the source at one of the microphone positions.

VIII. Future Work

Similarly to the work presented in this paper, we are studying sampling and interpolation of the sound field along circular microphone and loudspeaker arrays. These arrays are widely used in wave field synthesis and beamforming systems [11]. An application of our technique can be found in the sampling and interpolation of Head Related Transfer Functions (HRTFs) [22]. HRTFs are measured in anechoic chambers using circular arrays of loudspeakers. The representation of the 2D spectrum of the plenacoustic function also allows to derive in that case a sampling theorem to exactly define the number and necessary angular spacing between consecutive loudspeakers to reconstruct the HRTFs up to a particular temporal frequency [23].

IX. Conclusion

In this paper, we have introduced and studied the plenacoustic function. It characterizes the sound field at any point in space. We have studied this function and calculated its spectrum for the linear and the planar case without making any far field assumption. The decay of the spectrum has been studied along both the temporal and spatial frequency axis. Based on the support of the spectrum, we have determined the number and the spacing between the microphones needed to reconstruct the sound field up to a certain temporal frequency. The optimal sampling pattern for the microphone positions has also been given for the linear and the planar case. We analyzed how the decay of the spectrum influences the interpolation quality after sampling and reconstruction of the PAF. Finally, we presented simulations and experimental results and compared them with the theoretical results.

Appendix I

Derivation of the 2D-FT of the PAF on a line

Consider

$$p(x,t) = \frac{\delta(t - \frac{\sqrt{(x-x_s)^2+d^2}}{c})}{4\pi\sqrt{(x-x_s)^2+d^2}}. \tag{41}$$

The 2D-FT of (41) is

$$P(\phi,\omega) \quad = \quad \int_{x=-\infty}^{\infty}\int_{t=-\infty}^{\infty} \frac{\delta(t - \frac{\sqrt{(x-x_s)^2+d^2}}{c})}{4\pi\sqrt{(x-x_s)^2+d^2}} e^{-j(\phi x+\omega t)} \mathrm{d}t\mathrm{d}x$$

We call $u = x - x_s$, therefore

$$\begin{aligned} P(\phi,\omega) &= \frac{e^{-j\phi x_s}}{4\pi}\int_{u=-\infty}^{\infty}\frac{e^{-j(\phi u+\frac{\omega}{c}\sqrt{u^2+d^2})}}{\sqrt{u^2+d^2}}\mathrm{d}u \\ &= \frac{e^{-j\phi x_s}}{4\pi}\left\{\int_{u=0}^{\infty}\frac{e^{-j(\phi u+\frac{\omega}{c}\sqrt{u^2+d^2})}}{\sqrt{u^2+d^2}}\mathrm{d}u+\int_{u=0}^{\infty}\frac{e^{-j(-\phi u+\frac{\omega}{c}\sqrt{u^2+d^2})}}{\sqrt{u^2+d^2}}\mathrm{d}u\right\} \\ &= \frac{e^{-j\phi x_s}}{2\pi}\left\{\int_{u=0}^{\infty}\frac{e^{-j\frac{\omega}{c}\sqrt{u^2+d^2}}\cos(\phi u)}{\sqrt{u^2+d^2}}\mathrm{d}u\right\} \\ &= \frac{e^{-j\phi x_s}}{2\pi}\left\{\int_{u=0}^{\infty}\frac{\cos(\frac{\omega}{c}\sqrt{u^2+d^2})\cos(\phi u)}{\sqrt{u^2+d^2}}\mathrm{d}u-j\int_{u=0}^{\infty}\frac{\sin(\frac{\omega}{c}\sqrt{u^2+d^2})\cos(\phi u)}{\sqrt{u^2+d^2}}\mathrm{d}u\right\}. \end{aligned}$$

Using existing formula in [24], we obtain:

$$P(\phi,\omega) = -\frac{j}{4}e^{-j\phi x_s}H_0^*\left(d\sqrt{(\frac{\omega}{c})^2-\phi^2}\right).$$

APPENDIX II

DERIVATION OF THE 3D-FT OF THE PAF ON A PLANE

Consider

$$p(x_m,y_m,t) = \frac{\delta(t-\frac{a}{c})}{4\pi a},$$

with $a = \sqrt{(x_m-x_s)^2+(y_m-y_s)^2+(z_m-z_s)^2}$. We can calculate the spectrum of this function

$$\begin{aligned} P(\phi_x,\phi_y,\omega) &= \int_{x_m=-\infty}^{+\infty}\int_{y_m=-\infty}^{+\infty}\int_{t=-\infty}^{+\infty}\frac{\delta(t-\frac{a}{c})}{4\pi a}e^{-j(\phi_x x_m+\phi_y y_m+\omega t)}\mathrm{d}x_m\mathrm{d}y_m\mathrm{d}t \\ &= \int_{x_m=-\infty}^{+\infty}\int_{y_m=-\infty}^{+\infty}\frac{1}{4\pi a}e^{-j(\phi_x x_m+\phi_y y_m+\omega\frac{a}{c})}\mathrm{d}x_m\mathrm{d}y_m. \end{aligned}$$

We call $x = x_m - x_s$, $y = y_m - y_s$ and $z = z_m - z_s$. With these changes of variable we have that

$$P(\phi_x,\phi_y,\omega) = e^{-j(\phi_x x_s+\phi_y y_s)}\int_{x=-\infty}^{+\infty}\int_{y=-\infty}^{+\infty}\frac{1}{4\pi a}e^{-j(\phi_x x+\phi_y y+\omega\frac{a}{c})}\mathrm{d}x\mathrm{d}y.$$

We have that $a = \sqrt{x^2+y^2+z^2}$. We call $r^2 = x^2+y^2$, and $\phi_q^2 = \phi_x^2+\phi_y^2$. The integral can be rewritten as [25]:

$$P(\phi_x,\phi_y,\omega) = \frac{1}{2}e^{-j(\phi_x x_s+\phi_y y_s)}\int_{r=0}^{+\infty}\frac{r}{\sqrt{r^2+z^2}}J_0(\phi_q r)e^{-j(\omega\frac{\sqrt{r^2+z^2}}{c})}\mathrm{d}r.$$

Call $m = \sqrt{r^2+z^2}$, we have that $r = \sqrt{m^2-z^2}$, and also $\mathrm{d}m = \frac{r}{\sqrt{r^2+z^2}}\mathrm{d}r$. The integral becomes

$$P(\phi_x,\phi_y,\omega) = \frac{1}{2}e^{-j(\phi_x x_s+\phi_y y_s)}\int_{m=|z|}^{+\infty}J_0(\phi_q\sqrt{m^2-z^2})e^{-j(\omega\frac{m}{c})}\mathrm{d}m.$$

Using existing formulas in [24], we obtain that

$$P(\phi_x,\phi_y,\omega) = \begin{cases} \frac{-j}{2}e^{-j(\phi_x x_s+\phi_y y_s)}\frac{e^{-j|z|\sqrt{(\frac{\omega}{c})^2-\phi_q^2}}}{\sqrt{(\frac{\omega}{c})^2-\phi_q^2}} & \text{for} \quad |\phi_q| \le \frac{\omega}{c} \\ \frac{1}{2}e^{-j(\phi_x x_s+\phi_y y_s)}\frac{e^{-|z|\sqrt{\phi_q^2-(\frac{\omega}{c})^2}}}{\sqrt{\phi_q^2-(\frac{\omega}{c})^2}} & \text{for} \quad \frac{\omega}{c} \le |\phi_q|. \end{cases}$$

APPENDIX III
DERIVATION OF THE 4D-FT OF THE PAF IN SPACE

Consider

$$p(x_m, y_m, z_m, t) = \frac{\delta(t - \frac{a}{c})}{4\pi a},$$

with $a = \sqrt{(x_m - x_s)^2 + (y_m - y_s)^2 + (z_m - z_s)^2}$. We can calculate the spectrum of this function

$$\begin{aligned} P(\phi_x, \phi_y, \phi_z, \omega) &= \int_{x_m=-\infty}^{+\infty} \int_{y_m=-\infty}^{+\infty} \int_{z_m=-\infty}^{+\infty} \int_{t=-\infty}^{+\infty} \frac{\delta(t - \frac{a}{c})}{4\pi a} e^{-j(\phi_x x_m + \phi_y y_m + \phi_z z_m + \omega t)} \mathrm{d}x_m \mathrm{d}y_m \mathrm{d}z_m \mathrm{d}t \\ &= \int_{x_m=-\infty}^{+\infty} \int_{y_m=-\infty}^{+\infty} \int_{z_m=-\infty}^{+\infty} \frac{1}{4\pi a} e^{-j(\phi_x x_m + \phi_y y_m + \phi_z z_m + \omega \frac{a}{c})} \mathrm{d}x_m \mathrm{d}y_m \mathrm{d}z_m. \end{aligned}$$

We call $x = x_m - x_s$, $y = y_m - y_s$ and $z = z_m - z_s$. With these changes of variable we have that

$$P(\phi_x, \phi_y, \omega) = e^{-j(\phi_x x_s + \phi_y y_s + \phi_z z_s)} \int_{x=-\infty}^{+\infty} \int_{y=-\infty}^{+\infty} \int_{z=-\infty}^{+\infty} \frac{1}{4\pi a} e^{-j(\phi_x x + \phi_y y + \phi_z z + \omega \frac{a}{c})} \mathrm{d}x \mathrm{d}y \mathrm{d}z.$$

We have that $a = \sqrt{x^2 + y^2 + z^2}$. We call $\phi_s^2 = \phi_x^2 + \phi_y^2 + \phi_z^2$. The integral can be rewritten as [25]:

$$\begin{aligned} P(\phi_x, \phi_y, \phi_z, \omega) &= e^{-j(\phi_x x_s + \phi_y y_s + \phi_z z_s)} \int_{a=0}^{+\infty} \sin(\phi_s a) e^{-ja\frac{\omega}{c}} \mathrm{d}a \\ &= \frac{e^{-j(\phi_x x_s + \phi_y y_s + \phi_z z_s)}}{\phi_s^2 - (\frac{\omega}{c})^2}. \end{aligned}$$

APPENDIX IV
SPATIAL FREQUENCY DECAY OF THE PAF FOR LINES OF MICROPHONES NOT PARALLEL TO A WALL.

In this section, we consider the case of a line of microphones not parallel to a wall. The line of microphones is included in a plane that is parallel to the floor and the ceiling of the room. Two possible configurations will be studied: the case where the coefficient of direction of the line is rational or non-rational. For simplicity we consider in the rest of this section that $\frac{L_y}{L_x} \in \mathbb{Q}$.

1) The case of a line that has a rational coefficient of direction is first considered. In Fig. 18 a room is shown with all the virtual sources. The line where the field is to be studied follows a direction $\bar{g} = [g_x, g_y]$, with $\frac{g_y}{g_x}$ a rational number. It can be observed that the sound pressure measured on the distance denoted as L along $\bar{g}$ is enough to know the pressure on the whole line. This follows from the periodicity of the sources as shown in Fig. 18. To study the spatial decay of the spectrum of the PAF corresponding to this line, the same formalism as in Section III-A.2 is followed. Due to the periodicity L of the scheme, the spatial frequency of the spectrum is only defined for discrete values $n\phi_0$, with $\phi_0 = \frac{2\pi}{L}$.

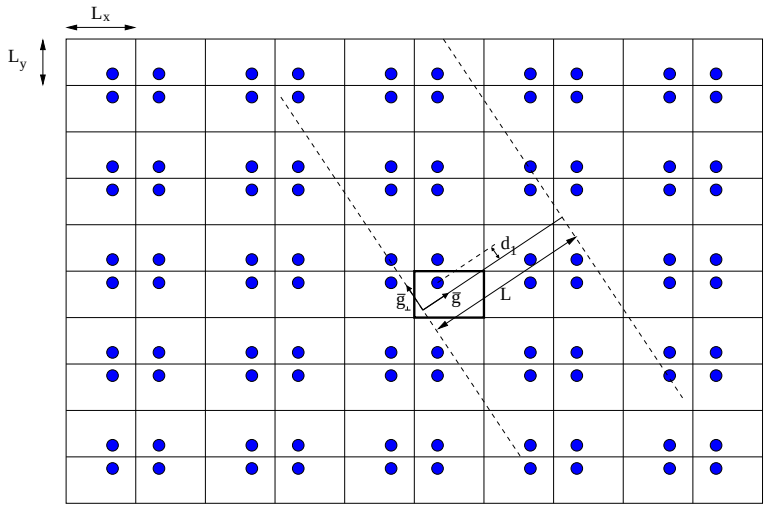

Fig. 18. a room is shown with its virtual sources. In the middle of the figure, the original room is shown in bold. A line with direction $\bar{g}$ is shown.

To obtain the spatial decay of the spectrum, one still needs to study the effect of the infinite number of sources in the region ranging from abscissa 0 to L along $\bar{g}$. One can remark that due to the rational character of $\bar{g}$, there exists a periodicity in the sources along the direction $\bar{g}_\perp$ being orthogonal to $\bar{g}$. This periodicity depends on the direction $\bar{g}$ but also on the size of the room. This periodicity is $L_p = \sqrt{(2\alpha L_x)^2 + (2\beta L_y)^2}$, with α and β the smallest possible integer numbers satisfying the relation

$$\frac{\alpha}{\beta} = \frac{-g_y L_y}{g_x L_x}.$$

Knowing this periodicity, the spectrum can easily be obtained similarly to the derivation of Section III-A.2. The only difference is that here more than four virtual sources need to be considered and that the periodicity L_y needs to be replaced by L_p. The final result is here also that

$$P(n\phi_0, \omega) = O(e^{-d_1 n \phi_0}),$$

with d_1 the distance between the closest source and the line of microphones.

Note that if the line passes through a source, $d_1 = 0$ and there is no more decay. This results corresponds to the fact that the Hankel function in (4) also goes to infinity in that case.

2) The case of a line having a non-rational coefficient of direction is now considered. In order to study the decay of the spectrum of the PAF on that line, one studies the decay of the spectrum of the plane that contains this line and that is also parallel to the ceiling and the floor of that room.

Further, by using the slice-projection theorem [25], one can study the spectrum corresponding to a specific line of the PAF (our line of interest). By observing the repetitions of the sources, one can observe that the PAF on the plane is periodic both in the x and in the y directions with periodicity $2L_x$ and $2L_y$ respectively. Therefore, the spectrum of the PAF is only defined for discrete values m and n with $\phi_{0x} = \frac{\pi}{L_x}$ and $\phi_{0y} = \frac{\pi}{L_y}$, $P(m\phi_{0x}, n\phi_{0y}, \omega)$. Without considering the periodicity, one can remark that the PAF spectrum can also be rewritten as:

$$P(\phi_x, \phi_y, \omega) = \sum_{m=-\infty}^{\infty} \sum_{n=-\infty}^{\infty} \delta(\phi_x - m\phi_{0x})\delta(\phi_y - n\phi_{0y})P(m\phi_{0x}, n\phi_{0y}, \omega). \tag{42}$$

In order to study the spectrum of the PAF along the line of interest, one needs to apply the projection-slice theorem. This theorem says that to study a slice of the PAF in time domain (in this case along the line of interest), one needs to project the spectrum along the corresponding line in frequency. Consider that the line of interest has a direction $\bar{g} = [g_x, g_y]$, the projection in the frequency domain will happen along the direction $\bar{g}_\perp = [-g_y, g_x]$ as shown in Fig. 19. Further, call ϕ_g the abscissa along the line G. Also, consider the lines $G_\perp(\phi_g)$ orthogonal to $\bar{g}$ and at positions ϕ_g on G. The spectrum of the PAF along the line of interest is given by:

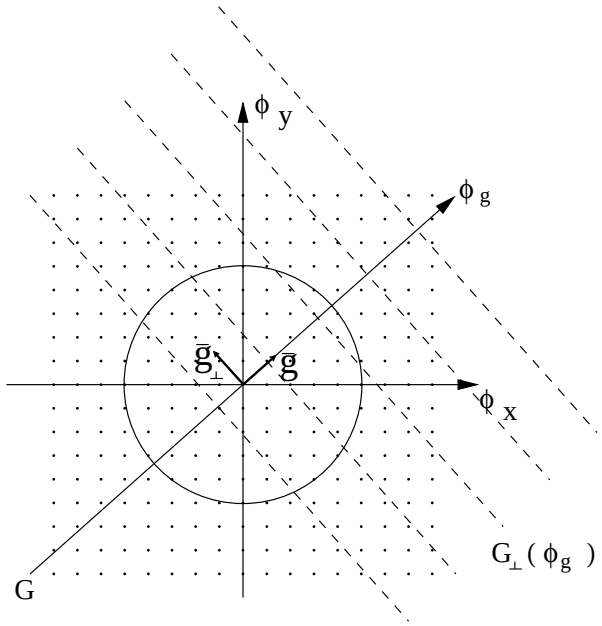

Fig. 19. Top view of the spectrum of the PAF for the plane of microphones. The spectrum is only defined for discrete values. The spectrum of the line of interest corresponds to the projection the spectrum of the PAF along directions $G_\perp$.

$$P_{\bar{g}}(\phi_g, \omega) = \int_{G_\perp(\phi_g)} P(\phi_x, \phi_y, \omega) \mathrm{d}s, \tag{43}$$

with s the abscissa along $G_\perp(\phi_g)$.

As $\frac{g_y}{g_x}$ is a non-rational value, it can be observed that every sample of the spectrum of the plane will be projected on distinct positions along G. When the source is in the same plane as the line of microphones, it was shown in (37) that the decay is not anymore exponential but becomes only linear. Therefore, in this case, the decay of the PAF spectrum will decay at least linearly. This decay is much slower than the one obtained in the case of a rational direction.

Nevertheless, when generalizing this study to 3 dimensions, whith sources also repeated along the z axis, the decay of the spectrum will be shown to become exponential at the condition that no sources would be located inside the plane of the microphones. We consider a plane of microphones parallel to the floor and the ceiling containing the line G and the original source with all its virtual sources outside of that plane. As shown in the image method [12], the original source is first repeated to create the 7 first virtual sources. Then, these 8 sources are further repeated with periodicity $2L_x$, $2L_y$ and $2L_z$ in the x, y and z directions respectively. Similarly to the 2-dimensional case, the PAF will be periodic along the x and y directions and therefore the PAF spectrum will be discrete in ϕ_x and ϕ_y. What differs from the 2-dimensional case, is that each of the 8 original sources to be considered is now repeated along the z axis with periodicity $2L_z$. For the simplicity of the calculations, we will only consider one of the 8 original sources and calculate the spectrum of the PAF for that source repeated in the 3 directions. It will then be shown that the other sources will be negligible when studying the decay for large spatial frequencies.

Due to the construction of the virtual sources, we have that among the 8 first sources, 4 will be located at distance z_1 from the plane of interest, with $z_1 \leq L_z$. The other 4 sources will be located at a distance $2L_z - z_1$ from the plane. Call s_1 one of the sources that is separated from the plane by a distance z_1. The spectrum of the PAF along the plane in the presence of s_1 without repetitions is (for large spatial frequencies):

$$P(m\phi_{0x}, n\phi_{0y}, \omega) = e^{-j(m\phi_{0x}x_s + n\phi_{0y}y_s)} \frac{e^{-z_1\Gamma(m,n)}}{2\Gamma(m,n)}, \tag{44}$$

with $\Gamma(m,n) = \sqrt{(m\phi_{0x})^2 + (n\phi_{0y})^2}$.

When considering s_1 with all its repetitions along the z axis, we obtain

$$\begin{aligned} P(m\phi_{0x}, n\phi_{0y}, \omega) &= e^{-j(m\phi_{0x}x_s + n\phi_{0y}y_s)} \sum_{i=-\infty}^{\infty} \frac{e^{-|z_1+2L_z i|\Gamma(m,n)}}{2\Gamma(m,n)} \\ &= \frac{e^{-j(m\phi_{0x}x_s + n\phi_{0y}y_s)}}{2\Gamma(m,n)} \sum_{i=0}^{\infty} \left(e^{-(z_1+2L_z i)\Gamma(m,n)} + e^{-(z_1'+2L_z i)\Gamma(m,n)} \right), \end{aligned}$$

with $z_1' = 2L_z - z_1$. We therefore can write that

$$P(m\phi_{0x}, n\phi_{0y}, \omega) = \frac{e^{-j(m\phi_{0x}x_s + n\phi_{0y}y_s)}}{2\Gamma(m,n)} \left(\frac{e^{-z_1\Gamma(m,n)}}{1 - e^{-2L_z\Gamma(m,n)}} + \frac{e^{(z_1-2L_z)\Gamma(m,n)}}{1 - e^{-2L_z\Gamma(m,n)}} \right).$$

Considering now, the other sources, we can observe that asymptotically for large m and n, the decay of the spectrum is of the following order:

$$P(m\phi_{0x}, n\phi_{0y}, \omega) = O\left(\frac{e^{-z_1\Gamma(m,n)}}{\Gamma(m,n)} \right). \tag{45}$$

It is thus shown that the PAF spectrum decays exponentially when studied in a 3-dimensional environment.

Here again, as $\frac{g_y}{g_x}$ is a non-rational value, it can be observed that every sample of the spectrum of the plane will be projected on distinct positions along G. Call $\phi_g(m_0, n_0)$ the abscissa of the projection of a specific point of the spectrum with coordinates (m_0, n_0). We have that $\phi_g(m_0, n_0) < \Gamma(m_0, n_0)$. As given by (45), we also know that the further we are from the center of the circle, the smaller is the value of the spectrum. This leads to the conclusion that $|P(\phi_g(m_0, n_0), \omega)| \leq |P(m_0\phi_{0x}, n_0\phi_{0y}, \omega)|$. Therefore we have that the projection of the PAF spectrum on G will decay at least as fast as (45).

Finally, once the spectrum of the infinite line is studied, one needs to perform a windowing of the spectrum to consider the fact that the sound field is only studied inside the room. This part happens similarily to the windowing in Section V.

APPENDIX V
TEMPORAL FREQUENCY DECAY OF THE PAF IN A RECTANGULAR ROOM.

We have

$$P(n_0\phi_0, \omega) \sim C_4(n\phi_0) \sum_{i=-\infty}^{\infty} \left(\frac{e^{-jD_{1,i}\frac{\omega}{c}}}{\sqrt{D_{1,i}\omega}} + \frac{e^{-jD_{2,i}\frac{\omega}{c}}}{\sqrt{D_{2,i}\omega}} \right).$$

We call $S_1(\omega) = C_4(n\phi_0) \sum_{i=-\infty}^{\infty} \frac{e^{-jD_{1,i}\frac{\omega}{c}}}{\sqrt{D_{1,i}\omega}}$ and $S_2(\omega) = C_4(n\phi_0) \sum_{i=-\infty}^{\infty} \frac{e^{-jD_{2,i}\frac{\omega}{c}}}{\sqrt{D_{2,i}\omega}}$. S_1 can be rewritten as:

$$\begin{aligned} S_1(\omega) &= \frac{C_4(n\phi_0)}{\sqrt{\omega}} \left(e^{-jd_1\frac{\omega}{c}} + \sum_{i=1}^{\infty} \frac{e^{-j\frac{\omega}{c}(d_1+2L_y i)}}{\sqrt{d_1+2L_y i}} + \sum_{i=-\infty}^{-1} \frac{e^{-j\frac{\omega}{c}|d_1+2L_y i|}}{\sqrt{|d_1+2L_y i|}} \right) \\ &= \frac{C_4(n\phi_0)}{\sqrt{\omega}} \left(e^{-jd_1\frac{\omega}{c}} + \sum_{i=1}^{\infty} \frac{e^{-j\frac{\omega}{c}(d_1+2L_y i)}}{\sqrt{d_1+2L_y i}} + e^{-jd_1'\frac{\omega}{c}} + \sum_{i=1}^{\infty} \frac{e^{-j\frac{\omega}{c}(d_1'+2L_y i)}}{\sqrt{d_1'+2L_y i}} \right) \end{aligned}$$

with $d_1^{'} = 2L_y - d_1$. Call the second and fourth terms of the previous expression $U_1(\omega)$ and $U_2(\omega)$ respectively. These two expression are shown to converge using the Dirichlet convergence test[14]. Considering $U_1(\omega)$, the Dirichlet convergence test can be applied[15] with $\{a_n\} = e^{-j\frac{\omega}{c}(d_1+2L_y i)}$ and $\{b_n\} = \frac{1}{\sqrt{d_1+2L_y i}}$. This proves the convergence of $U_1(\omega)$. Similarily, it can also be shown that $U_2(\omega)$ converges. Furthermore, $U_1(\omega)$ and $U_2(\omega)$ are periodic function of ω. Therefore, they can be upperbounded and are converging for all possible values of ω. This leads us to the conclusion that $S_1(\omega)$ behaves asymptotically as

$$S_1(\omega) = \frac{C_5(\omega)}{\sqrt{\omega}},$$

with $C_5(\omega)$ a bounded function of ω. We obtain the same result for $S_2(\omega)$ and therefore we have that

$$P(n_0\phi_0, \omega) \sim \frac{C(\omega)}{\sqrt{\omega}},$$

with $C(\omega)$ a bounded function of ω.

Similarly to the derivations of Appendix IV, the derivation can be generalized when the line of microphones is not parallel to a wall.

REFERENCES

[1] E. Adelson and J. Bergen, "The plenoptic function and the elements of early vision," in *Computational Models of Visual Processing*. MIT Press, 1991, pp. 3–20.

[2] J. Chai, X. Tong, S. Chan, and H. Shum, "Plenoptic sampling," in *Proceedings of the conference on Computer graphics*, 2000, pp. 307–318.

[3] C. Zhang and T. Chen, "Generalized plenoptic function," Carneggie Mellon University, Tech. Rep. 01-06, September 2001.

[4] M. Kubovy and D. Van Valkenburg, "Auditory and visual objects," *Cognition*, vol. 80, pp. 97–126, 2001.

[5] T. Ajdler and M. Vetterli, "The plenacoustic function and its sampling," in *IEEE Benelux Workshop on Model Based Processing and audio Coding*, 2002.

[6] ——, "The plenacoustic function, sampling and reconstruction," in *Proc. of IEEE ICASSP*, 2003.

[7] ——, "Acoustic based rendering by interpolation of the plenacoustic function," in *SPIE/IS&T Visual Communication and Image Processing Conference*, 2003.

[8] A. Berkhout, *Applied Seismic Wave Theory*. Elsevier Science, 1987.

[9] J. Coleman, "Three-phase sample timing on a wideband triangular array of 4/3 the usual density reduces the nyquist rate for far-field signals by two thirds," in *The 38th Annual Asilomar Conference on Signals, Systems, and Computers, Pacific Grove CA, USA*, 2004.

[14]Let $\{a_n\}$ and $\{b_n\}$ be sequences of real numbers such that $\{\sum_{i=0}^{n} a_i\}$ is bounded and $\{b_n\}$ decreases with 0 as limit. Then $\sum_{n=0}^{\infty} a_n b_n$ converges.

[15]In this case we have to split the exponential in a_n in its sine and cosine expression to be able to apply the convergence test since it was defined for real expressions.

[10] D. de Vries and M. Boone, “Wave field synthesis and analysis using array technology,” in *IEEE Workshop on Applications of Signal Processing to Audio and Acoustics, New Paltz, New York*, 1999.

[11] E. Hulsebos, D. de Vries, and E. Bourdillat, “Improved microphone array configurations for auralization of sound fields by wave field synthesis,” in *110th AES Convention*, 2001.

[12] J. B. Allen and D. A. Berkley, “Image method for efficiently simulating small-room acoustics,” *J. Acoust. Soc. Am.*, vol. 65, 1979.

[13] P. M. Morse and K. U. Ingard, *Theoretical Acoustics*. New York McGraw-Hill, 1968.

[14] E. G. Williams, *Fourier Acoustics*. Academic Press, 1999.

[15] T. Ajdler, L. Sbaiz, and M. Vetterli, “The plenacoustic function and its sampling,” Ecole Polytechnique Federale de Lausanne, Tech. Rep., 2004.

[16] M. Vetterli and J. Kovačević, *Wavelets and Subband Coding*, ser. Signal Processing. Prentice Hall, 1995.

[17] P. Vaidyanathan, *Multirate systems and filter banks*. Prentice Hall, 1992.

[18] J. Coleman, “Ping-pong sample times on a linear array halve the nyquist rate,” in *IEEE ICASSP*, 2004.

[19] S. Müller and P. Massarani, “Transfer function measurement with sweeps,” *J. Audio Eng. Soc.*, vol. Vol 49, 2001.

[20] G. Elko, E. Diethorn, and T. Gänsler, “Room impulse response variation due to thermal fluctuation and its impact on acoustic echo cancellation,” in *IWAENC*, kyoto, 2003, pp. 67–70.

[21] T. Theußl, T. Möller, and E. Gröller, “Optimal regular volume sampling,” in *IEEE Visualization*, 2001.

[22] J. Blauert, *Spatial hearing*. MIT press, 2001.

[23] T. Ajdler, L. Sbaiz, and M. Vetterli, “The plenacoustic function on the circle with application to HRTF interpolation,” *Accepted to IEEE ICASSP*, 2005.

[24] I. S. Gradshteyn and I. M. Ryzhik, *Table of Integrals, Series, and Products*, 4th ed. New York: Academic Press, 1965.

[25] R. N. Bracewell, *The Fourier Transform and its Applications*. McGraw-Hill, 2000.